PROMPT FISSION NEUTRON INVESTIGATION IN THERMAL NEUTRON INDUCED FISSION

Sh. Zeynalov, P. Sedyshev, V. Shvetsov, O. Sidorova

Joint Institute for Nuclear Research, Dubna, Russia

Abstract. The prompt neutron emission in thermal neutron induced fission of ^{235}U has been investigated applying digital signal electronics. The goal was to compare the results of our digital data acquisition and digital signal processing analysis to the results of the pioneering work of Apalin et al. Using a twin Frisch grid ionization chamber for the fission fragment detection and a NE213 equivalent neutron detector in total about 10^6 neutron coincidences have been registered. The fission fragment kinetic energy, mass and angular distribution has been investigated along with prompt neutron time of flight and pulse shape using a six channel synchronous waveform digitizer with sampling frequency of 250 MHz and 12 bit resolution. The signals have been analyzed using digital pulse processing algorithms, developed by authors.

Keywords: neutron induced fission, ^{235}U, prompt fission neutron emission, neutron multiplicity, fission fragment mass distribution, total kinetic energy distribution**.**

1. Introduction

The nuclear fission is considered as the process of charged drop development under competition between attractive nuclear and repulsing coulomb forces, leading eventually to the split of the nucleus mainly into two parts of comparable masses. The main part of fission fragments (FF) excitation energy is released by the prompt fission neutrons, emitted by FF after full acceleration by coulomb forces. The experimental investigations of various characteristics of PFN emission is needed to understand the nuclear fission dynamics from the scission point down to rupture. One of the interesting observation is the increasing $\bar{\nu}(A)$ from the heavy fragment with increase of the excitation energy of the fissioning system [1] still has no clear explanation. Therefore, further systematic studies of correlations between fragment+neutron characteristics are needed. The studies of PFN emission in fission induced by neutrons from energies extending from resonances up to a few MeV could possibly contribute to better understanding the mechanism of PFN emission from the excited FF. The experiments on sub-barrier fission, induced by thermal neutrons are of particular interest because of no measurements were done so far on mass and energy distributions for this systems [2]. In this work we report preliminary results of PFN investigation thermal neutron-induced fission of ^{235}U. The main goal of the experiment was the feasibility check of the apparatus and data analysis procedure.

2. Experimental Setup and FF data analysis

A convenient way to study of PFN emission in neutron-induced fission is to use a conventional twin back-to-back ionization chamber, with two chambers sharing a common

cathode as was done by Budtz-Jorgensen and Knitter [3]. The cathode is made from a thin conductive foil and at the same time serves as backing for the fissile deposit. For binary fission events two complementary FF are simultaneously detected in two independent chambers. Free electrons released by FF deceleration are induced pulses on the chambers anodes and on the common cathode during drift along the applied externally electric field. The pulse height in each chamber was proportional to corresponding FF kinetic energy release and the FF pulse shape conveys information on the FF angle (Θ) in respect to the electric field applied in the direction of the normal to the cathode plane. From the correlated energies obtained in the above double-energy (2E) experiment, FF masses and velocities could be found in the way similar to that in book [4]. If the fissile target is located on the common cathode and the fast neutron detector positioned at the certain distance along the normal to the target the angle between FF and PFN emission would be equal to Θ. The PFN velocity may be determined from the known flight path and the measured time delay between cathode and ND pulses. Measured FF and PFN velocity vectors then may be used for PFN emission kinematics. The PFN multiplicity distributions in respect to FF kinetic energy release and mass split may be reconstructed by comparison of two sets of FF measurements. In the first experiment fission fragment mass and kinetic energy release should be evaluated from the measurement independent from ND. In the second experiment FF mass and kinetic energy release should be evaluated for the FF coincided with ND. The detailed information on PFN emission in fission is available from the measured dependence of the number $\nu(A,TKE)$ of PFN emitted by the FF with mass number A and TKE release of two fission fragments [3–4]. The late function allows obtaining of averaged characteristics on $\bar{\nu}(A)$ or $\bar{\nu}(TKE)$ by integrating over respective variable, if the mass yield matrix - *Y(A,TKE)* is known, for example:

$$\bar{\nu}(A)=\frac{\int_0^\infty \nu(A,TKE)Y(A,TKE)dTKE}{\int_0^\infty Y(A,TKE)dTKE},\quad \bar{\nu}=\int_0^\infty \nu(A,TKE)Y(A,TKE)dTKEdA,\quad 200=\int_0^\infty Y(A,TKE)dTKEdA \qquad (1)$$

Similar relation could be written for averaging over A:

$$\bar{\nu}(TKE)=\frac{\int_0^\infty \nu(A,TKE)Y(A,TKE)dA}{\int_0^\infty Y(A,TKE)dA},\quad \bar{\nu}=\int_0^\infty \nu(A,TKE)Y(A,TKE)dTKEdA,\quad 200=\int_0^\infty Y(A,TKE)dTKEdA \qquad (2)$$

$\nu(A,)$, $\nu(TKE)$ can be easily determined if the distributions of $P(A,TKE)$ and $Y(A,TKE)$ are known. The experimental method and data analysis procedure implemented in this work was adopted from Ref. [3], where it was described in detail. For each fission event the FF and PFN kinetic energies, FF masses along with the angle between PFN and FF motion should be determined. All this information can then be used to reconstruct the PFN emission kinematics both in the laboratory (LF) and in the centre of mass (CMF) frames. The measurements were carried out using the experimental setup presented in the left side of Fig. 1. Reaction kinematics is sketched in the right of Fig. 1. The experimental setup consists of the twin back-to-back ionization chamber (TIC), which was designated for FF kinetic energy release and the cosine of angle between fission axis and the cathode plane normal measurement. The

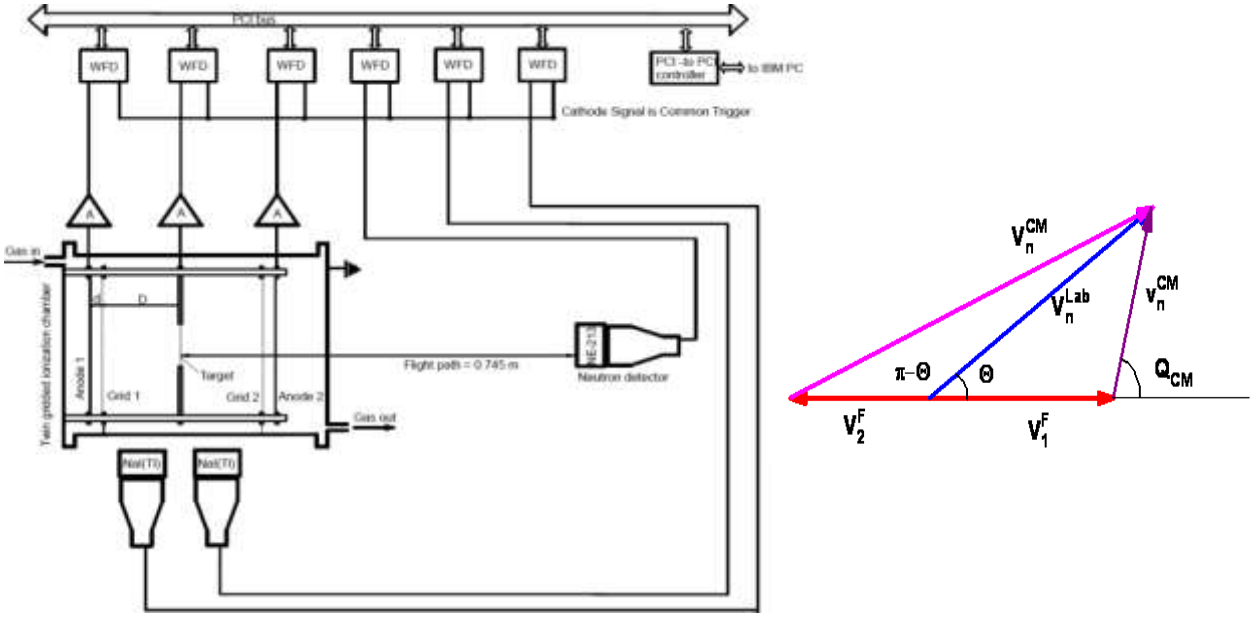

FIGURE 1. Experimental setup (on the left). Vector diagram for PFN emission from FF (on the right).

experimental data was collected using a digital pulse processing (DPP) system, consisting of six synchronous waveform digitizers (12 bit, 250 MS/sec). The FF energies and angles were obtained from the chamber signal waveforms using DPP, realized in form of recursive procedures. The neutron energy was derived from the time-of-flight (TOF) calculated as delay between the cathode and the neutron detector pulses. The measured FF energy release should be corrected for energy losses in the target layer and target backing if the cosine of angle Θ is known. In this work anode current pulse waveform was derived from the output pulse of charge sensitive preamplifier and the pulse "centre of gravity" (T) calculated as described in Ref. [5]. The relation between T and the cos(Θ) was derived in Ref. [6] using Ramo-Shokley theorem and numerically calculated weighting potentials:

$$\cos(\Theta) = (T_{90} - T)/(T_{90} - T_0), \tag{3}$$

where the used variables have the following meaning: D is the cathode-anode distance, d is the grid–anode distance, σ is the Frisch grid inefficiency, T_0=T(cos(Θ)=1), T_{90}=T(cos(Θ)=0). The below formula was used to correct anode signal pulse heights for grid inefficiency:

$$P_A^C = P_A/(1-\sigma(1-\frac{T}{T_{90}})\cdot(1+\frac{d}{2D})) \tag{4}$$

Once the emission angle is calculated the average anode pulse height versus 1/cos(Θ) was plotted for both chambers to find energy loss correction for FF detected in each chamber as demonstrated in Fig. 2b. The data sets are fitted as a linear function of 1/cos(Θ), the slopes of which were assigned to energy loss correction in respective chamber. The correction for FF pulse height caused by momentum transfer to working gas atoms by FF (non ionizing collisions) during its deceleration – is called pulse height defect (PHD). The PHD depends on

the FF mass and kinetic energy and was corrected in data analysis using parameterization suggested in Ref. [7]:

$$PHD(A_{post}, E_{post}) = \frac{A_{post} \cdot E_{post}}{\alpha} + \frac{A_{post}}{\beta}, \quad (5)$$

where E_{post}, A_{post} – FF kinetic energy and mass respectively after neutron emission. The fitting parameters α and β are chosen to arrive at the values of TKE and $\langle A_H \rangle$ as given in Ref. [4] p. 323. After all corrections have been implemented we went to reconstruct the mass yield for investigated reaction. To do so we needed $\bar{\nu}(A)$ from literature and we used data from Ref. [8] and from Ref. [2]. The mass yield curve was obtained using $\bar{\nu}(A)$ for ^{235}U(n_{th},f) reaction from Ref. [2] is shown in Fig. 4 in comparison with result $\bar{\nu}(A)$ published in Ref. [4] p. 300.

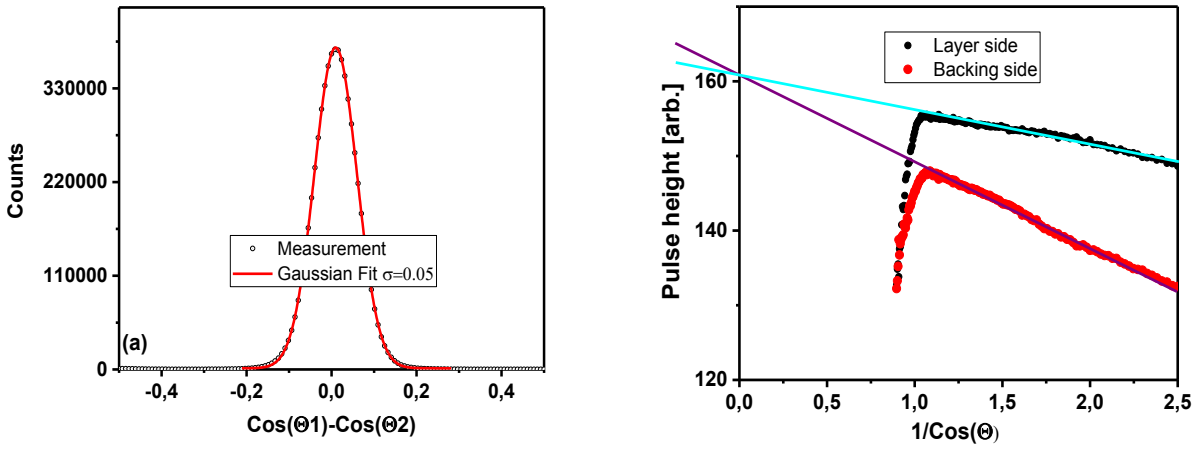

FIGURE 2. (a) Precision of cos(Θ) measurement. (b) The energy-loss correction factors determined as the slopes of the linear fit of function of the mean pulse height on 1/cos(Θ).

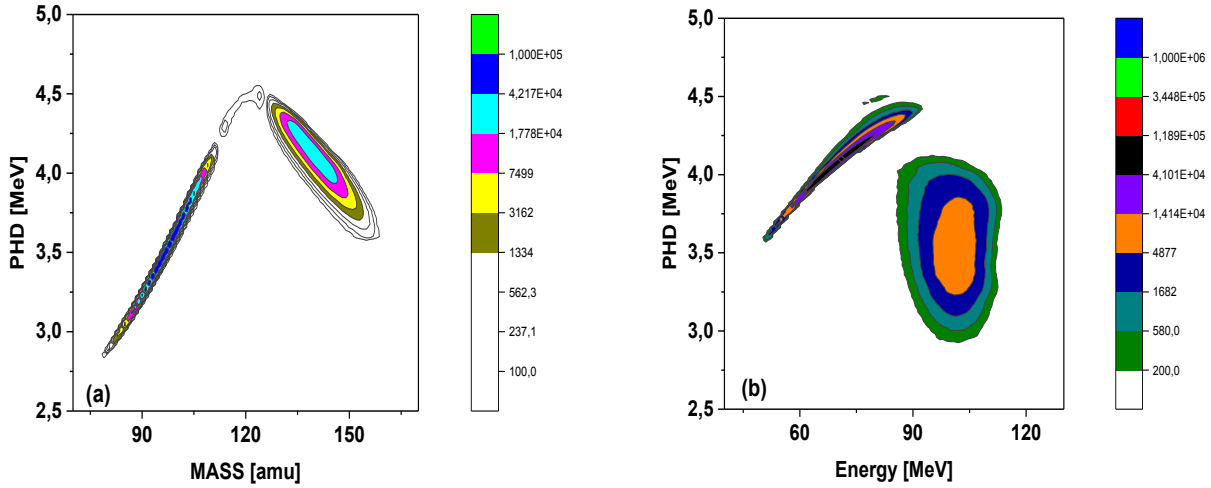

FIGURE 3. (a) Dependence of PHD correction on FF mass. (b) Dependence of PHD correction on FF kinetic energy. Both the dependences taken from the three dimensional function PHD(A,E) constructed from experimental data.

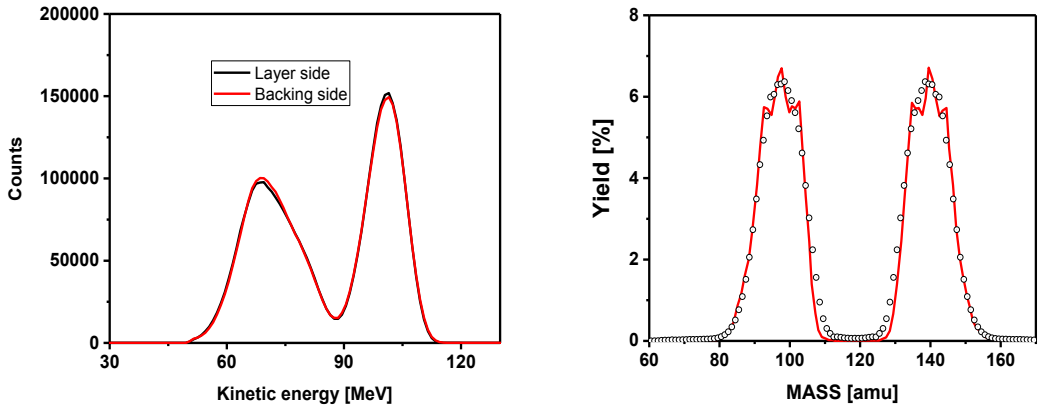

FIGURE 4. (a) FF kinetic energy distribution after all corrections were applied and linear energy calibration scale with two parameters implemented to set the TKE=170.5 MeV and the light FF kinetic energy set to 100.6 MeV. (b) Comparison of measured mass yield (dots) with data (solid line) taken from Ref.[4], p. 300. For calculations the successive approximation procedure to obtain pre-PFN emission mass described in Ref. [3] was used.

3. PFN data analysis

Measurement of PFN time-of-flight in present experiment was done using cathode pulse of TIC as a "T-zero" signal and the ND signal as "Stop" signal. The signals were digitized with 250 MHz sampling rate and stored during experiment for further off-line data analysis. Time difference between these two signals was analyzed implementing standard constant fraction time marking (CFTM) algorithm both to the cathode and to the ND waveforms. The realization of the algorithm demonstrated in Fig. 5(a) as it was applied to the cathode waveform. The copy of the original signal is delayed by approximately 0.4 of the cathode signal rise time (~1000 ns) and summed with scaled and inverted original signal. The "T-zero" time is assigned to the crossing point of resulting signal with time axis. The crossing point was calculated using parabola interpolation between two successive samples, first of which has positive and second the negative values. The time mark for the ND signal was found in the similar way. It should be noted that to achieve the best timing resolution in CFTM realization one should convert sampled waveform to continuous form using Shannon's sampling formula [9]. Unless we do not deal with energy spectrum reconstruction, the resolution (~2.5 ns) provided in this simple implementation we found sufficient for PFN analysis. The neutron multiplicity is estimated by counting the number of coincidence between cathode pulse and PFN signal of ND. Due to high gamma radiation background both from the target and surrounding materials the PFN counts need to be separated from the gamma radiation using pulse shape analysis as described in Ref. [9] p. 679. FIG. 6(a) demonstrates the result of two integral methods implemented in our experiment. FIG. 6(b) demonstrates the efficiency of pulse shape analysis for separation PFN from the background gamma-radiation. The PFN detected by ND mainly is emitted from FF moving towards the ND, but the probability, that it was emitted by FF moving in opposite direction (complementary FF) is not zero and these events should be considered as the background. The background created by the complementary FF was investigated in Ref. [5] and was slightly modified in our approach.

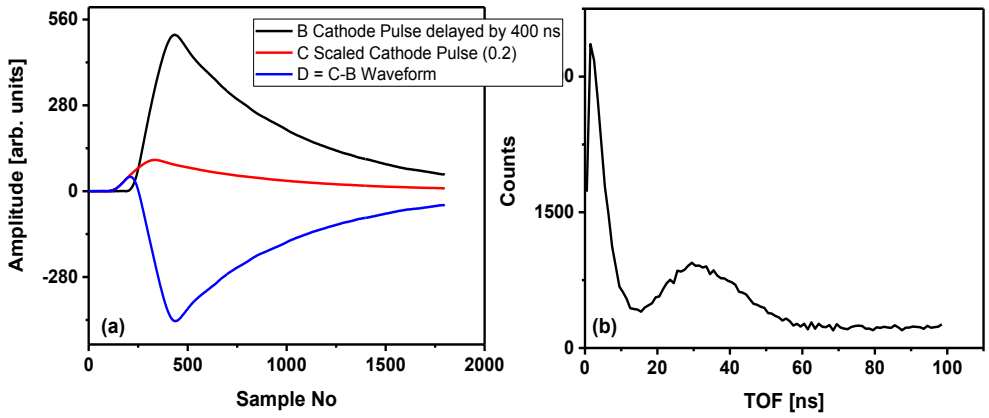

FIGURE 5. (a) Demonstration of digital CFTM realization for ionization chamber cathode signal. (b) Measured PFN time-of-flight distribution measured using digital CFTM.

According to the reaction kinematics depicted in fig. 1 (right), the kinetic energy of the second FF in the CMF, must be much higher than the kinetic energy of the first FF. Bearing in mind the exponential drop of the PFN energy spectrum in the CMF, the contribution to the PFN from both FFs could be evaluated using the probabilities defined as:

$$W_x = 1 \; W_y = \exp(E^x_{CM} - E^y_{CM}), \tag{5}$$

where W_x, W_y - are probabilities of PFN emission with CM kinetic energies $E^{x,y}_{CM}$ of FF and its complement respectively, the parameter N is a normalization factor. A comparison of the mass distributions plotted using measured data and probabilities, defined by eq. (5) are presented in fig. 7a. Results are similar to ref. [3], where the background from the complementary fragments for ^{252}Cf(SF) was found to be small.

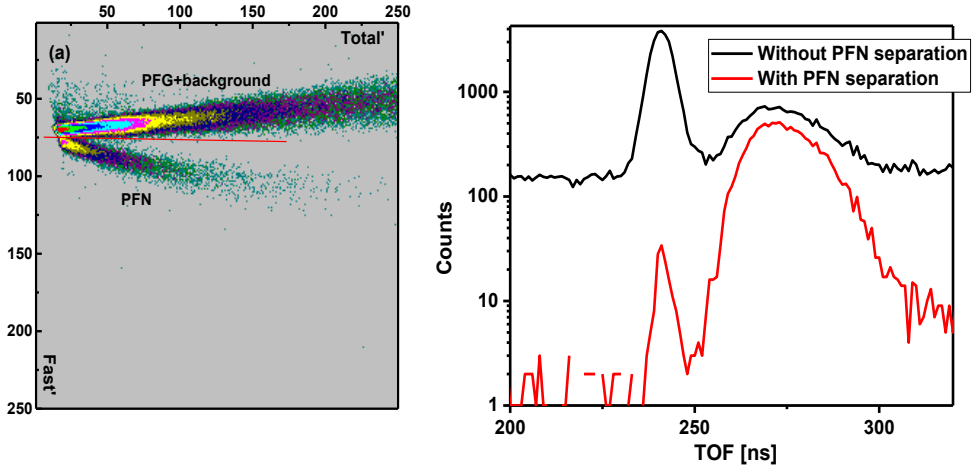

FIGURE 6. (a) Demonstration of pulse shape separation efficiency with help of two integral method [10]. (b) PFN time-of-flight distribution before and after pulse shape analysis applied and background was subtracted.

The angular distribution of PFN emitted in FF CM reference frame is plotted in fig. 7b, proving that almost all of the PFN are emitted from fully accelerated FFs. The transformation from the LAB to CM reference frame was done using the following formula:

$$\int_0^{\infty} v_{CM} F(v_{CM}, \cos(\Theta_{CM}))dv_{CM} = \int_{V_L \cos(\Theta) > V_{FF}}^{\infty} v_L N(v_L, \cos(\Theta))dv \qquad (6)$$

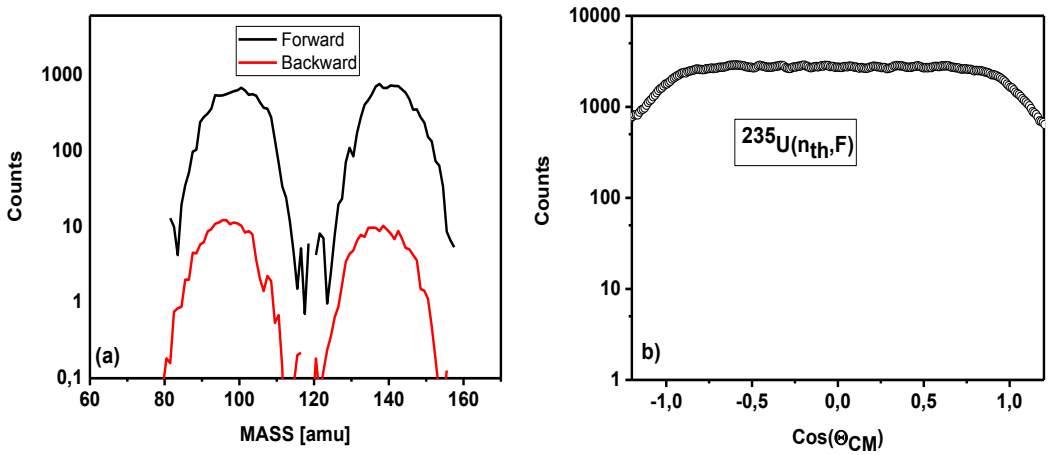

FIGURE 7. (a) Demonstration of the background level from the complementary FF to investigated PFN distribution. (b) The angular distribution of PFN emission measured in the FF CM frame.

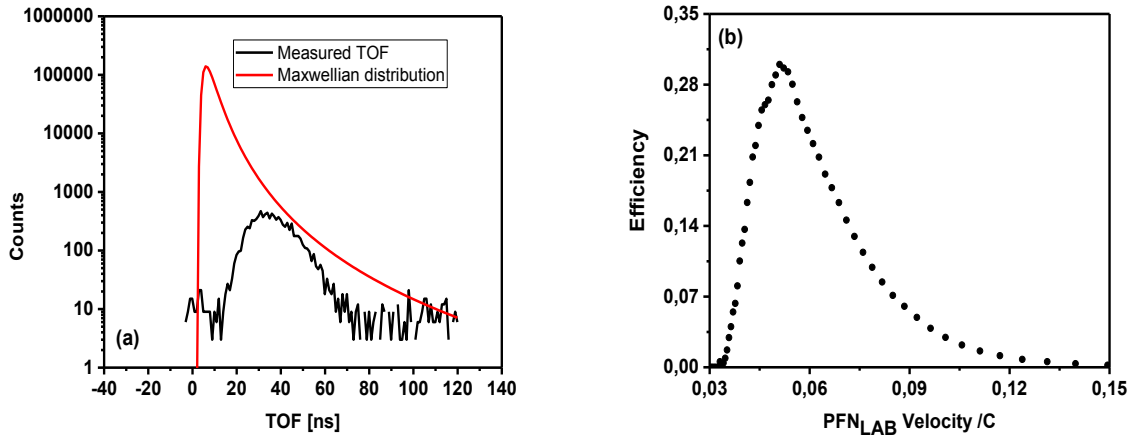

FIGURE 8. (a) Comparison of PFN Maxell distribution calculated for the flight path of 0.65 m with temperature parameter 1.313 MeV and $\bar{\nu} = 2.44$ with measured TOF in one out of 7 measurements. (b) The ND efficiency -ε, evaluated from comparison with Maxell distribution and averaged over all measurements. Velocity is given as the ratio to C= speed-of-light.

4. PFN distribution evaluation from the measured data

The PFN distribution was evaluated considering neutron emission from the fully accelerated FF and using the reference frame moving along with the FF towards the ND. We used the Jacobian factor and conversion formulae from CM to LAB reference frame from the Ref. [11] as follows:

$$\bar{\nu}(A,TKE)=\int_0^{\infty}\frac{Yc(A,TKE,V_{LAB})\bullet V_{CM}\bullet(V_{LAB}-V_F\bullet\cos(\Theta))}{\varepsilon(V_{LAB})\bullet V_{LAB}^2}dV_{LAB}\,/\,Y(A,TKE), \tag{7}$$

where $Y_C(A,TKE,V_{LAB})$ – the number of FF coincidences with ND, $\varepsilon(V_{LAB})$ is the ND efficiency dependence on PFN velocity in LAB frame, V_{LAB} – the PFN velocity measured in LAB frame, V_F – FF fragment velocity in LAB frame, V_{CM} is the PFN velocity in CM frame. The distribution $Y(A,TKE)$ calculated without demanding coincidence with ND as was described above, but distribution $Yc(A,TKE,V_{LAB})$ calculated with FF energy corrections as was described in Ref. [12].

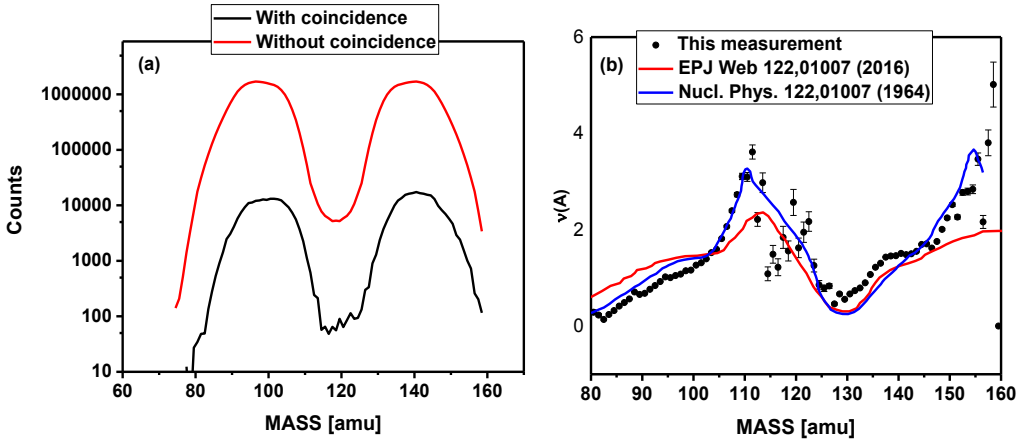

FIGURE 9. (a) Mass distributions of FF measured without (red line) demanding coincidence with ND and with coincidence (black line). (b) The average PFN emission distribution dependence on FF mass in comparison with literature data.

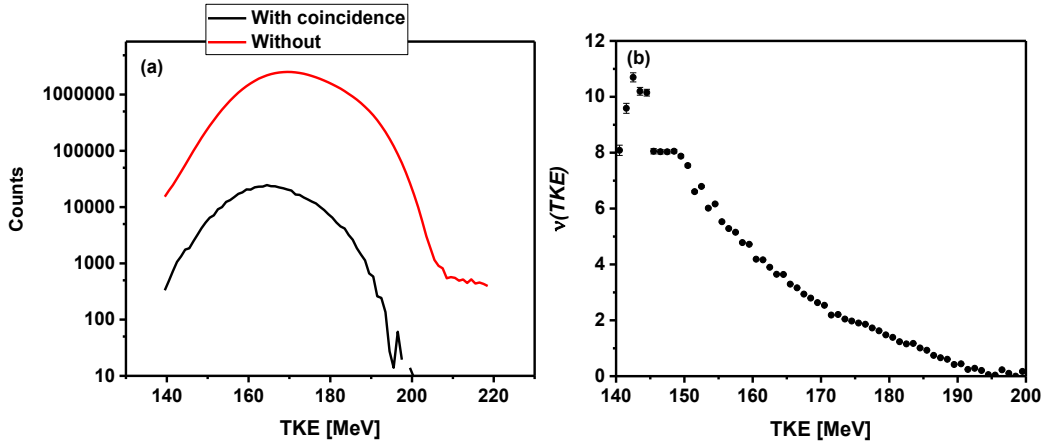

FIGURE 10. (a) TKE distributions of FF measured without (red line) demanding coincidence with ND and with coincidence (black line). (b) The average PFN emission distribution dependence on FF total kinetic energy value.

References

1. A.A. Naqvi, F. Kappeler, and F. Dickmann, Phys. Rev. C**34**,218 (1986).
2. A. Al-Adili, D. Tarrio, F.-J. Hambsch, A. Gook, K. Jansson, A. Solders, V. Rakopoulos, C. Gustavson, M. Lantz, A. Materrs, S. Oberstedt, A.V. Prokofiev, M. Viladi, M. Osterlund, and S. Pomp, EPJ Web of Conferences 122,01007 (2016).
3. C. Budtz-Jorgensen and H.-H. Knitter, Nucl. Phys., A**490**, 307 (1988).
4. C. Wagemans, The Nuclear Fission Process, CRC Press, Boca Raton , FL, 1991.
5. S. Zeynalov, O. Zeynalova, F.-J. Hambsch and S. Oberstedt, Bull. Russ. Acad. Sci.: Phys. **73**,506 (2009).
6. Zeynalov Sh., Jaksybekov A., Sedyshev P., Sidorova O., Shvetsov V. XXIV International Seminar on Interaction of Neutrons with Nuclei, Dubna, May 23-27, 2016, JINR to be published.
7. F.-J. Hambsch, J. van Aarle, and R. Vogt, Nucl. Instrum. and Meth. A361, 257 (1995).
8. V.F. Apalin, Yu. N. Gtitsuk, I.E. Kutikov, V.I. Lebedev, and L.A. Mikaelyan, Nucl. Phys., **55**, 249 (1964).
9. O. Zeynalova, Sh. Zeynalov, M. Nazarenko, F.-J. Hambsch, and S. Oberstedt, AIP Conf. Proc. 1404, 325(2011).
10. G. Knoll, Radiation Detection and Measurement, John Willey & Sons, Inc, Third edition, 2001.
11. H.R. Bowman, J.C.D. Milton, S.G. Thompson, and W.J. Swiatecki, Phys. Rev. **129** (1963) 2133.
12. A. Gavron, Nucl. Instrum. and Meth., **115** (1974) 99.